

Infall of galaxies onto groups

M. V. Santucho^{1,2}, M. L. Ceccarelli^{1,2} and D. G. Lambas^{1,2}

¹Instituto de Astronomía Teórica y Experimental (IATE), CONICET-UNC, Laprida 854, X5000BGR, Córdoba, Argentina
e-mail: santucho@oac.unc.edu.ar

²Observatorio Astronómico de Córdoba (OAC), Universidad Nacional de Córdoba (UNC), Córdoba, Argentina.

Received ; accepted

ABSTRACT

Context. Growth of the structure in the Universe manifest as accretion flows of galaxies onto groups and clusters. Thus, the present day properties of groups and their member galaxies are influenced by the characteristics of this continuous infall pattern. Several works both theoretical, in numerical simulations, and in observations, study this process and provide useful steps for a better understanding of galaxy systems and their evolution.

Aims. We aim at exploring the streaming flow of galaxies onto groups using observational peculiar velocity data. The effects of distance uncertainties are also analyzed as well as the relation between the infall pattern and group and environment properties.

Methods. This work deals with analysis of peculiar velocity data and their projection on the direction to group centers, to determine the mean galaxy infall flow. We applied this analysis to the galaxies and groups extracted from the Cosmicflows–3 catalog. We also use mock catalogs derived from numerical simulations to explore the effects of distance uncertainties on the derivation of the galaxy velocity flow onto groups.

Results. We determine the infalling velocity field onto galaxy groups with $cz < 0.033$ using peculiar velocity data. We measure the mean infall velocity onto group samples of different mass range, and also explore the impact of the environment where the group reside. Well beyond the group virial radius, the surrounding large-scale galaxy overdensity may impose additional infalling streaming amplitudes in the range 200 to 400 km/s. Also, we find that groups in samples with a well controlled galaxy density environment show an increasing infalling velocity amplitude with group mass, consistent with the predictions of the linear model. These results from observational data are in excellent agreement with those derived from the mock catalogs.

Key words. Techniques: radial velocities – Galaxies: clusters: general –large-scale structure of Universe

1. Introduction

In the nearby Universe, galaxy peculiar velocities manifest the evolution of the large-scale structure. This growth of structure, within hierarchical clustering scenarios, cause the increase of the masses of galaxy groups and clusters through the continuous accretion of smaller systems. Thus, the galaxy velocity field of the infalling regions of clusters is expected to contain a significant radial infall component superposed to other orbits with larger angular momentum content.

The spherical infall model (Regos & Geller 1989) describes the dynamical behavior of objects surrounding isotropic overdense regions with a collapsing velocity field whose amplitude depends on the distance (r) to the local overdensity (Diaferio & Geller 1997). Peebles (1976, 1980) derived a linear approximation to the velocity field induced by an isotropic mass overdensity (δ) and the predicted infall velocity is $V_{inf}^{linear} = -1/3 H_0 \Omega_0^{0.6} r \delta(r)$, where Ω_0 is the density parameter and H_0 is the Hubble constant at present.

However, a pure spherical infall model cannot correctly predict the amplitude of the velocity field since in this model the amplitude of the velocity field depends on local conditions and not on the surrounding mass distribution.

Peculiar velocities arise through galaxy motions departing from a pure Hubble flow induced by the gravitational potential of mass overdensities distributed at large scales, so that global conditions are needed to fully describe the velocity field around a mass concentration.

Observationally, the effects of peculiar motions can be reliably inferred statistically via redshift-space distortions (hereafter RSD) studies (Croft et al. 1999; Padilla et al. 2001; Ceccarelli et al. 2006; Paz et al. 2013; Cai et al. 2016). Besides, peculiar velocities can also be measured directly and used in other ways to extract useful information on the dynamics of galaxies and galaxy systems.

It should be recalled that peculiar velocity measurements directly trace the mass distribution, avoiding the complications of galaxy bias, present in RSD (Desjacques & Sheth 2010). These measurements comprise a large range of scales and also may be used to add information on the nature of gravity by comparison to other modeling of galaxy motions.

For the mentioned reasons, the evolution of large structures can be constrained either by direct measurements of peculiar velocities or by the effects of redshift space distortions. Galaxy peculiar velocities generated by mass irregularities are superimposed to the cosmological expansion so that it can be easily inferred from its redshift and a redshift independent distance estimation. Along these lines, galaxy peculiar velocities are gaining interest as a promising cosmological probe that provides new information on the dynamics of galaxies and systems at low redshift (Johnson et al. 2014; Huterer et al. 2017; Dupuy et al. 2019; Adams & Blake 2020; Kim & Linder 2020). Tonegawa et al. (2020) analyze redshift–space distortions in clustering measures to constrain cosmological parameters and examine the satellite velocity bias between galaxies and dark matter inside haloes. Recent works reconstruct peculiar velocities and the associated

density fields using Cosmicflows-3 data. Their results highlight the ability of peculiar velocities to probe the mass distribution and reveal under/over-dense structures in the Local Universe (Graziani et al. 2019).

Several authors have performed studies of the streaming motions at large and intermediate scales using peculiar velocities (in regions that extent up to $\approx 100 h^{-1} \text{Mpc}$). In these studies, the bulk flow amplitude derived from the observational velocity field is often compared to the predictions of the standard Λ CDM cosmological model (Watkins et al. 2009; Lavaux et al. 2010; Feldman et al. 2010; Colin et al. 2011; Nusser & Davis 2011; Turnbull et al. 2012; Ma & Pan 2014).

In this work we study the accretion of galaxies onto groups using the peculiar velocity field derived from redshift-independent distance measurements and analyze the infall amplitude dependence on mass group and surrounding galaxy density environment. We also analyze the effects of anisotropies of the large scale galaxy distribution on the infall velocity fields onto groups.

This paper is organized as follows, in section 2 we introduce the data sets used, in section 3 we describe the statistical method implemented to obtain the mean infall amplitude from observational peculiar velocities. In section 4 we display and analyze our results on infall onto groups using simulated and observational data respectively. In section 5 we assess anisotropies on infall velocities. In section 6 we examine local effects vs large scale environment on infall. Finally, in section 7 we summarize and discuss our results.

2. Data

2.1. Observational data

The Cosmicflows-3 catalog (CF3) comprises almost 18,000 distances of galaxies and is the largest compilation of redshift independent extragalactic distances available (Tully et al. 2016). This catalog is based on the two previous versions, providing distances derived by the authors own observations as well as estimates extracted from the literature, homogenized to the same scale system. Galaxy distances provided in the catalog are obtained from different methods, eg luminosity–linewidth (Tully-Fisher) relation, the Fundamental Plane (FP), surface-brightness fluctuations, Type Ia super-nova (SNIa) observations, etc. Nearby galaxy distances are accurate at the level of 5-10 %. However, at larger distances the uncertainties raise up to 20-25 %.

In this work, we use the online version of the CF3 consisting of data for groups of galaxies as well as individual galaxies with no association to groups. While the catalog include groups identified over the full redshift range of the 2MRS survey (Huchra et al. 2012), following the advice in Tully et al. (2016), we only considered the groups with velocities between 3,000 and 10,000 km^{-1} , since the properties of the nearest and farthest groups are uncertain. It is worth to mention that a group can have multiple contributions and therefore their distance uncertainty are reduced by averaging over all data source.

The group catalog also includes masses estimated from the virial theorem and derived from the integrated K_s band luminosity (Tully 2015). It is well known that applying the virial theorem provides a poor estimate of group masses when these systems have a low number of members, while estimates of group masses through their total luminosities may provide more suitable proxies to the actual masses (see Eke et al. (2004)). In addition, we

highlight that only groups with at least 5 group members have mass estimates derived from the virial theorem. For this reason, we use mass estimates derived from the integrated K_s band luminosity throughout the paper. In figure 1 we display the sky distribution of high and low mass groups, according to the median group mass value (red and blue circles for $M > 3.4 \times 10^{13} M_\odot$ and $M < 3.4 \times 10^{13} M_\odot$ respectively). As it can be noticed, both distributions trace large scale structures in a similar fashion. Further details of group catalog can be found on Tully (2015); Tully et al. (2016).

The CF3 provides measurements of redshifts and distance moduli so that galaxy peculiar velocities, not explicitly included may be derived through:

$$v_{pec} \approx (v_{mod} - H_0 d) / (1 - v_{mod}) \quad (1)$$

where v_{mod} is the velocity with respect to the Cosmic Microwave Background corrected for cosmological effects (Tully et al. 2013). The calibration of CF3 distances is set by the choice of the fiducial value of $H_0 = 75 \text{ km s}^{-1}$. Tully et al. (2016) shows that this value minimizes the monopole term with CF3 distances and results in a small global radial infall and outflow in the peculiar velocity field. For these reasons, we use this value in our analysis.

As it is well known, due to observational uncertainties that increase with distance, peculiar velocities can take unrealistic values. For this reason, we have removed from our analysis galaxies with relative distance errors larger than 20 % and peculiar velocities larger than 1500 km s^{-1} ($|v_{pec}| > 1500 \text{ km s}^{-1}$). With these restrictions, the samples considered in this work comprise 2180 galaxies and 657 galaxy groups. This sample extracted from the CF3 is called hereafter CF3S. In table 1 we summarize the galaxy and group samples used here and their main characteristics. The first two lines correspond to the CF3S galaxy and group samples previously described. The following lines contain information on the group subsamples selected for the analyses carried out in this work and are introduced in the corresponding sections.

2.2. Mock catalogs

In order to compare model predictions to observational results we used mock catalogs based on galaxies extracted from the semi-analytical model presented by Henriques et al. (2015). This catalog include 2MASS photometric bands which are also in the group catalog supplement in CF3. This semi-analytical model is an update of the Munich galaxy formation model consistent with the first-year Planck cosmology (Planck Collaboration et al. 2011), including a new treatment of baryonic processes to reproduce recent data on the abundance and passive fractions of galaxies from $z=3$ down to $z=0$. Henriques et al. (2015) use the Millennium Simulation (Springel et al. 2005), which follows structure formation in a box of side $500 h^{-1} \text{Mpc}$ comoving with a resolution limit of $8.6 \times 10^8 h^{-1} M_\odot$. The cosmological parameters used in this semi-analytical model correspond to the first-year Planck, $\sigma_8=0.829$, $H_0=67.3 \text{ km s}^{-1} \text{Mpc}^{-1}$, $\Omega_\Lambda = 0.685$, $\Omega_m = 0.315$, $\Omega_b=0.0487$.

We have constructed 25 mock catalogs in order to compare model predictions to observational results and examine possible biases generated by systematic errors in the observational data. Each of these mock catalogs have a Hubble parameter $H_0=75 \text{ km s}^{-1}$ consistent with the Cosmicflows-3 catalog and are used to estimate the effect of cosmic variance on our results. The

set of mocks mimic as much as possible the characteristics of the observational catalogs. In order to reproduce the statistical properties of the observations we place an observer inside the simulation box, and consider a volume representative of the observational volume. The same angular mask as the observational catalog is applied, excluding an area similar to that produced by the extinction of our galaxy's disk (Zone of Avoidance). The galaxies are selected at random in such a way to obtain comparable number density of galaxies with a similar redshift distribution. In addition, the mock catalogs are also designed to reproduce the current observational measured distances and their estimated uncertainties.

We use haloes identified with a 'friends of friends' (FOF) algorithm with standard parameters (Henriques et al. 2015). We select those FoF halos imposing a similar mass distribution as the observations. These restrictions provide suitable samples to test the dynamics of infalling semianalytic galaxies onto these mass inhomogeneities, resembling the infall of galaxies onto groups in the real universe.

Large uncertainties of distance measurements strongly affect the derived radial peculiar velocities and uncertainties can be as large as the peculiar velocities. In addition, distance estimates are subject to systematic biases, as homogeneous and inhomogeneous Malmquist biases (Strauss & Willick 1995; Dekel 1994), that can generate spurious artifacts in the inferred velocity field. We have analyzed and quantified the impact of uncertainties of distance measures on the infall mean velocity determination by assigning errors to the mock catalogs similar to those affecting the observational data

In general, the different distance indicators have a fractional distance uncertainty. Primary distances estimators such as the tip of the giant branch, cepheids, or surface brightness fluctuations give distances with relative errors up to 5% – 10% whereas secondary indicators, reach uncertainty estimates up to 25%.

As it is well known, uncertainties in redshift independent galaxy distance estimates are consistent with a Gaussian distribution in distance moduli. As a consequence of this behavior, uncertainties of both, distance and peculiar velocity are expected to have a log-normal distribution. In order to assess the effects of these distance uncertainties on our results, we have assumed a gaussian distribution of errors in distance moduli, with mean and dispersion as derived from the CF3, ie. consistent with a mean relative distance uncertainty of 17%. These uncertainties are used to modify the distances of each galaxy in the mock catalog $d_n = d \times 10^{f_d}$, where f_d is taken from a Gaussian distribution. These mock catalogs are called hereafter mock-biased catalogs, while mock catalogs with no errors in galaxy distances, mock-unbiased catalogs.

The left panel of figure 2 displays both distance distribution for the CF3S and for a typical random mock with modified distances (mock-biased). As it can be seen in this figure both distribution are similar, providing confidence on our assumptions to assign distance uncertainties in simulated data. The radial peculiar velocities computed from equation 1 are shown in the right panel. Dashed lines correspond to the CF3S and dotted-dashed line to the mock-biased. In order to highlight how distance errors introduce biases in radial peculiar velocities we show in the same panel the distribution of the velocities for the same mock with error free distances (mock-unbiased). The distributions related with CF3S and mock-biased reveal a skewness towards negative peculiar velocities and both are flatter than the mock-unbiased. This effect is a consequence of the asymmetry in the distribution of fractional errors on distance, skewing peculiar velocity mea-

surements to negative values. Regarding comparison between distances and peculiar velocities, there is a qualitatively good agreement between CF3S and mock-biased catalog. The galaxies from the mock-biased catalog are distributed consistently with observations.

3. A statistical approach to derive the mean infall component of galaxy peculiar velocities onto groups

From the dynamical point of view, galaxy groups can be idealized as spherical, isolated mass overdensities. Under this simplified approximation, the expected peculiar velocity field of galaxies in groups and in their surroundings results from the sum of a spherical infall component plus a random velocity dispersion induced by the virialization of the central region. This picture is consistent with linear theory where convergent velocity fields may be directly associated to spherical isolated mass overdensities in a cosmological substratum.

Given the limitations of the observations where only the line-of-sight projection (LOS) of the peculiar velocity of galaxies can be estimated, the derivation of the observed velocity field associated to the infall onto groups depends on the position of the galaxy relative to both, the group center and the observer (see equation 2). Then, for galaxies at relative distance r to the group, the infall amplitude ($V_{inf}(r)$) can be derived from the LOS peculiar velocity (V_{pr}) by the lineal relation shown in equation 2,

$$V_{pr}(r, \theta) = V_{inf}(r) \cos(\theta) \quad (2)$$

where θ is the angular separation between the galaxy and the observer as seen from the group center.

In order to derive $V_{inf}(r)$, we consider galaxies located at different spherical concentric shells of radius r around the groups. For each shell we examine the dependence of the peculiar velocity on $\cos(\theta)$. Then, for different $\cos(\theta)$ bins we calculate the average galaxy peculiar velocity $\langle V_{pr} \rangle$, removing iteratively the galaxies whose peculiar velocity lie at more than $1.5\sigma_{V_{pr}}$ from the mean derived for each bin with the data used in the previous iteration. The mean infall amplitude $V_{inf}(r)$ can be simply derived by applying a least-squares linear fit to the $(\cos(\theta), \langle V_{pr} \rangle)$ vs group-centric radius r .

Note that in the reference system adopted, positive velocities correspond to infall motions while outflow velocities have negative values in our convention.

3.1. Recovering the mean infall amplitude in simulated data

The comparison between the mean infall amplitudes as a function of r obtained by averaging the peculiar velocities and those derived from equation 2 allows for a reliability test of our methods. For this aim, we take advantage of the information provided by synthetic catalogs, in particular the three-dimensional and the LOS peculiar velocities.

We explore the dependence of the peculiar velocity on $\cos(\theta)$ in the mock-unbiased catalogs and apply a least-squares linear fit to $(\cos(\theta), \langle V_{pr} \rangle)$. We show some examples of this relation in the four panels at the left of figure 3, where each panel corresponds to different group-centric distance range, as indicated in the figure, where the slopes of the linear fits are displayed in the small upper boxes in each panel. These slopes correspond to the derived mean infall amplitudes and are used to generate the infall curve shown in the right panel of this figure.

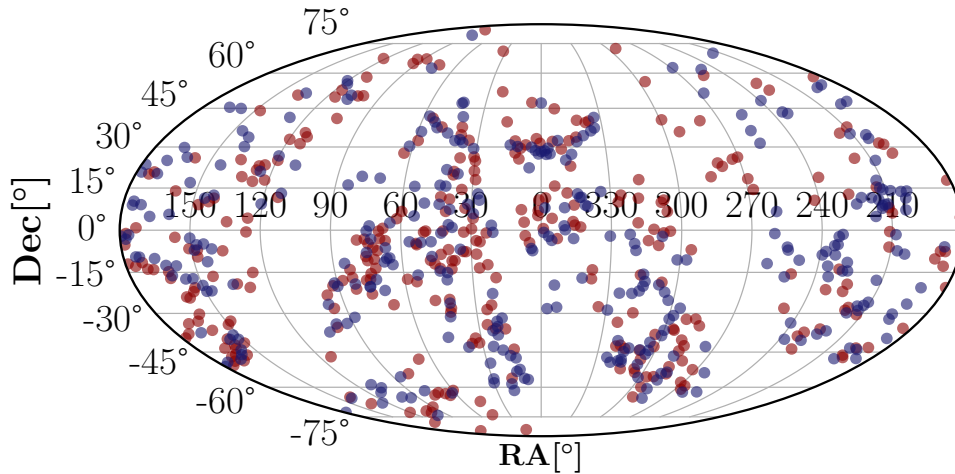


Fig. 1. Sky distribution of galaxy groups in equatorial coordinates. Color codes correspond to high/low mass groups, $M > 3.4 \times 10^{13} M_{\odot}$ (red circles), and $M < 3.4 \times 10^{13} M_{\odot}$ (blue circles) respectively.

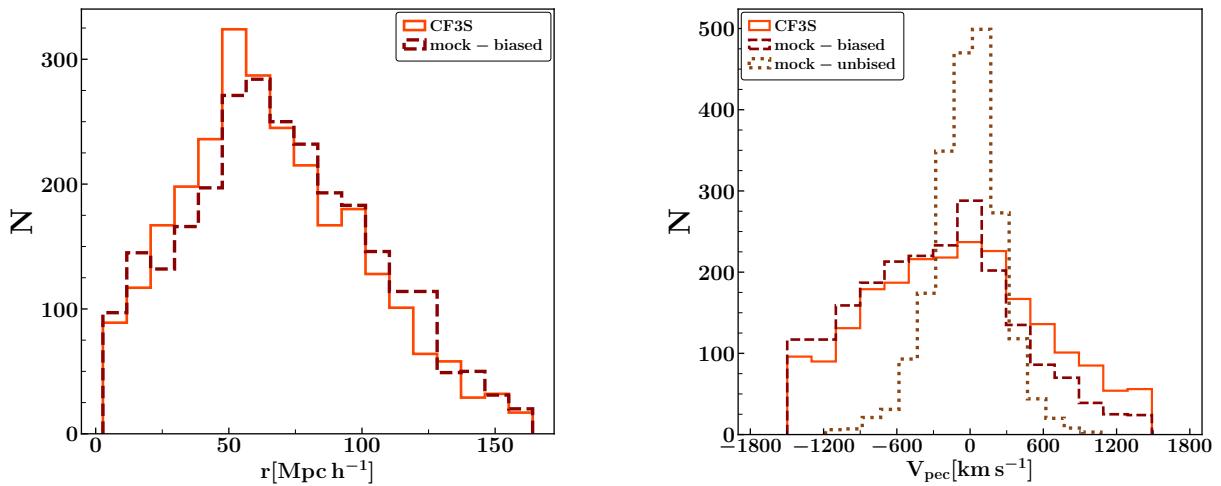


Fig. 2. Left panel: Distributions of distances in the Cf3S (solid orange line) and in a typical mock catalog with distance errors included (mock-biased, dashed brown line). Right panel: Distribution of radial peculiar velocities in the CF3S (solid line histogram) and in the mock biased catalogs (dashed histogram). A large tail towards negative values is observed in both distributions. The distribution associated to the mock catalog without errors (mock-unbiased, dotted brown line histogram) has a nearly Gaussian radial peculiar velocity distribution.

We derive the mean infall amplitude $V_{inf}(r)$ as a function of distance to the group for the 25 mock catalogs and in the upper right panel of the figure 3 we show the results averaged over the 25 mock-unbiased catalogs. The solid line denotes the mean infall motion derived from the projection of the three-dimensional velocity vector ($V_{mock-unbiased}(3d)$) along the group-centric direction, whereas the dashed line corresponds to the mean infall velocity ($V_{mock-unbiased}$) inferred by the procedure described in section 3 and shown in the left panels.

Uncertainties are derived from the scatter of measurements obtained from the 25 mock-unbiased catalogs, consistent with a suitable measure of cosmic variance.

As it can be seen in upper right panel of figure 3, the mean infall velocity estimate via the three-dimensional vector (solid line) and those inferred from LOS peculiar velocities (dashed line) are in excellent agreement, indicating that the proposed statistical method allows to derive the mean infall velocities from peculiar velocities.

We notice a convergent velocity field onto groups which can be clearly distinguished up to group-centric distances of 18 Mpc

h^{-1} , showing large scale flows of galaxies directed onto groups. Closer to group centres, the mean infall velocity reaches a maximum of approximately 200 km s^{-1} , where the effects of the potential well associated to the groups dominates the local radial infall. At larger distances the velocity field is no longer dominated by the group mass concentration but rather obeys the surrounding large scale structure, implying an average decline of the mean infall velocity.

The shaded region in the lower right panel of figure 3 shows the dispersion of the ratio between the actual mean group-centric infall velocity and the mean infall velocities derived from peculiar velocities for each mock-unbiased. As we can see there is a suitable agreement between the two measures which provides confidence in our method in deriving reliable infall amplitude determinations.

4. Observed velocity field around groups

Once we have tested the reliability of our methods to assess the effects of LOS projection of peculiar velocity in the

Table 1. Summary of the main characteristics of groups and galaxy samples.

| sample | object | selection criteria | mass range [M_{\odot}] | vel range [km s^{-1}] | Number |
|---------------------------|----------|--------------------------|---|----------------------------------|--------|
| CF3S | galaxies | | | 100–15000 | 2180 |
| all | groups | | $[2 \times 10^{12} - 5.5 \times 10^{14}]$ | 3000–10000 | 657 |
| HM | groups | group mass | $> 3.4 \times 10^{13}$ | 3000–10000 | 328 |
| LM | groups | group mass | $< 3.4 \times 10^{13}$ | 3000–10000 | 329 |
| direction | | | | | |
| \parallel overdensities | groups | large scale anisotropies | \parallel LOS | 3000–10000 | 296 |
| \perp overdensities | groups | large scale anisotropies | \perp LOS | 3000–10000 | 361 |
| overdensity range | | | | | |
| high density | groups | overall galaxy density | > 4 | 3000–10000 | 150 |
| intermediate density | groups | overall galaxy density | 2–4 | 3000–10000 | 225 |
| low density | groups | overall galaxy density | 0–2 | 3000–10000 | 271 |

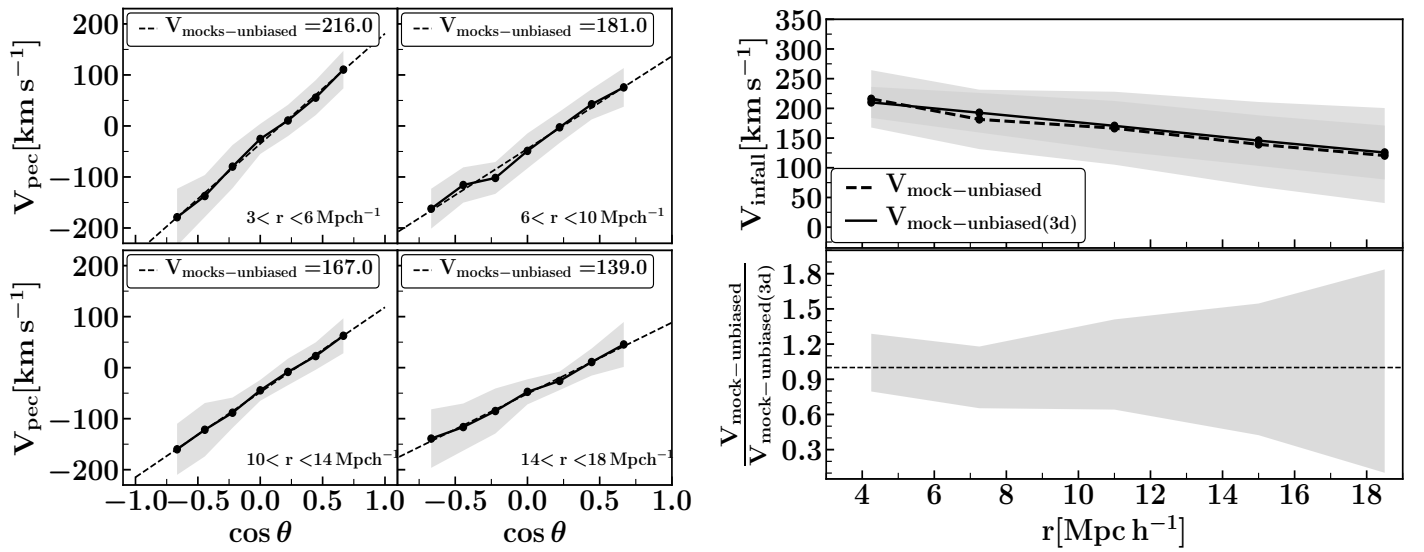


Fig. 3. Left figure: Mean peculiar velocity as a function of the angle the galaxy–group and group–observer directions (θ) in the mock–unbiased catalogs. Each panel correspond to a different galaxy–group distance, as is indicated in the figure. The dashed line indicates the best linear fitting, the slope is associated to the infall amplitude ($V_{\text{mock-unbiased}}$) and it is specified in each panel. The gray region correspond to the peculiar velocity dispersion. Right figure, upper panel: Mean infall velocity as a function of distance to the group center in the mock–unbiased catalogs. Solid line indicates the mean velocity directly obtained from the 3-dimensional peculiar velocity ($V_{\text{mock-unbiased(3d)}}$). Dashed line corresponds to the infall amplitude ($V_{\text{mock-unbiased}}$) obtained by applying our statistical method at LOS peculiar velocities and coincides with the slopes of the lines in the left figure. The displayed velocities are averaged over 25 mock–unbiased catalogs and the shadow region shows their dispersion. Right figure, lower panel: Dispersion of the ratio between the mean infall velocities $V_{\text{mock-unbiased(3d)}}$ and the mean infall $V_{\text{mock-unbiased}}$ velocities for each mock–unbiased

mock–unbiased catalogs, we study here the streaming infall flow around groups. For this aim we use observed peculiar velocity data applying our analysis to the samples of galaxies and groups described in section 2.

We derive the mean streaming velocity toward groups in the observational data by applying the same procedures used in the mock–unbiased catalogs (section 3.1). In figure 4 we show the mean projected peculiar velocity as a function of $\cos(\theta)$ bins for the samples of galaxies and groups taken from the CF3S (points) and their best linear fitting (dashed lines). The different panels correspond to spherical shells at different distances (r) to the groups, as indicated in the figure. In this figure, uncertainties are derived from the scatter of measurements obtained from the CF3S (error-bars), and gray shadow regions correspond to the

dispersion of results obtained in 25 mock–biased catalogs. We acknowledge the very good agreement between the results of the mock–biased catalogs and the observations, totally consistent within uncertainties.

As it can be seen, we obtain positive slopes consistent with a neat infall (see the small panels in the right of the figure) for all the distance ranges analyzed. Thus, our results show a clear signal for infall onto groups. Moreover, by inspection to this figure it can be noticed that the dispersion around the mean infall velocity is larger in the inner group–centric distance bin (upper left panel of the figure 4) possibly due to the contribution of motions from the virialized and pre–virialized regions (Diaferio & Geller 1997; Diaferio 1999). Beyond this scale the mean projected peculiar velocity become more stable and errors get smaller, show-

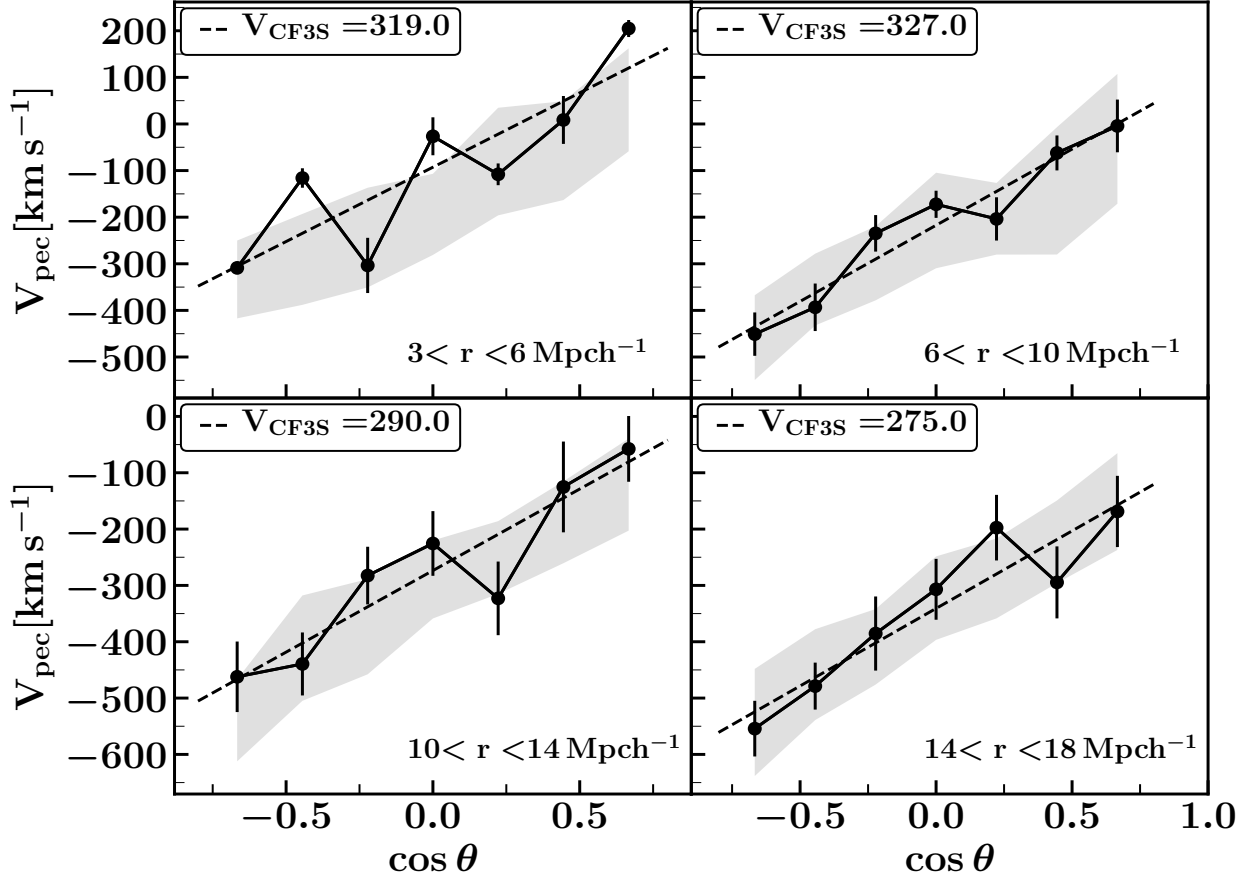


Fig. 4. Mean peculiar velocity as a function of the angle between the directions galaxy-group and group-observer (θ) in the CF3S (points). Each panel correspond to a different galaxy-group distance, as is indicated in the figure. The dashed line indicates the best linear fitting, the slope is associated to the *infall* amplitude (V_{CF3S}) and it is specified in each panel. The error-bars correspond to the peculiar velocity dispersion. The gray shaded areas encloses the dispersion of mean peculiar velocity from 25 mock-biased catalogs. Notice that the range of y-axis in upper and lower panels is different.

ing the expected smoother flow from large distances. At larger scales the influence of surrounding structures starts to affect the infall pattern and the systematic radially inward velocities decreases. This behavior is expected at large scales where the infall signal becomes negligible due to the presence of the gravitational pull of neighboring groups, clusters and filaments (notice the different peculiar velocity ranges of the upper and lower panels).

This behavior could be a consequence of biases that affect CF3S distances resulting in spurious velocity flows (Tully et al. 2016). Even more, the radial peculiar velocity distribution has a negative skewness, as shown in figure 2, and this asymmetric bias could contribute to obtain large negative peculiar velocities. It is worth to notice that mock-biased catalogs present the same behavior (gray shaded areas) while mock-unbiased do not show this trend.

In figure 5, we show the resulting mean velocity infall as a function of group-centric distance, $V_{\text{infall}}(r)$ for CF3S, (V_{CF3S} , dot-dashed lines), as derived from the linear fit applied to each panel of figure 4. We also show in this figure the results from mock LOS peculiar velocities with ($V_{\text{mock-biased}}$) and without ($V_{\text{mock-unbiased}}$) errors included (dashed and solid lines respectively).

It can be seen that when distance uncertainties are included, the mean infall velocity corresponding to mock-biased catalogs, agree well with those derived from CF3S data (dot-dashed and

dashed lines respectively). By inspection to figure 5 it can be seen that V_{CF3S} infall flow (dashed line) reaches a maximum of approximately 300 km s^{-1} , which is 50% larger when compared to the infall flow from mock-unbiased catalogs (solid line).

As it is evident from this analysis, a proper address of distance uncertainties is crucial in deriving reliable peculiar velocity fields around groups.

4.1. Correcting for distance uncertainties effect on infall determination

The resulting average group-centric infall velocities recovered from the mock catalogs are used to calibrate and correct the observational results.

In order to correct for the effect of distance uncertainties in the inferred infall velocities, we compare the results from the mock catalogs with and without the inclusion of errors (mock-biased and mock-unbiased respectively). We calculate the ratio $f = V_{\text{mock-biased}} / V_{\text{mock-unbiased}}$, where $V_{\text{mock-biased}}$ is the infall amplitude of the mock catalogs with distance errors (see dashed line in figure 5) and $V_{\text{mock-unbiased}}$ is the infall amplitude from the mock catalogs without distance uncertainties (see solid lines in figure 5).

A fitting function of the form $f = ar^2 + br + c$ is sufficient to provide a good description of the ratio of observed to actual velocities. We find that the parameters $a = 1.2$, $b = 0.05$, $c = -0.0002$

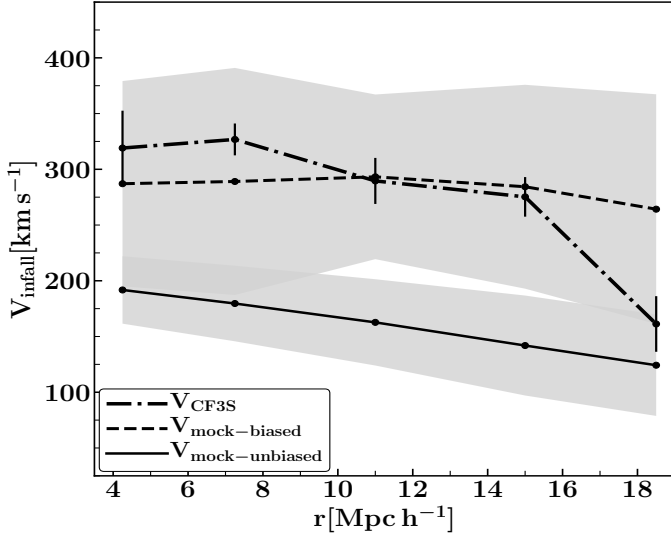


Fig. 5. Mean infall velocity as a function of distance to the group center for biased samples. Dashed line indicates the mean velocity obtained from the mock with errors included (mock-biased), and the dot-dashed line corresponds to Cosmicflows-3 sample (CF3S). For comparison we include the mean infall velocity for mock-unbiased (solid line). Error bars correspond to the uncertainty in the mean infall velocities from CF3S. The shaded region indicates the variance obtain from 25 mock without (with) errors included catalogs realizations.

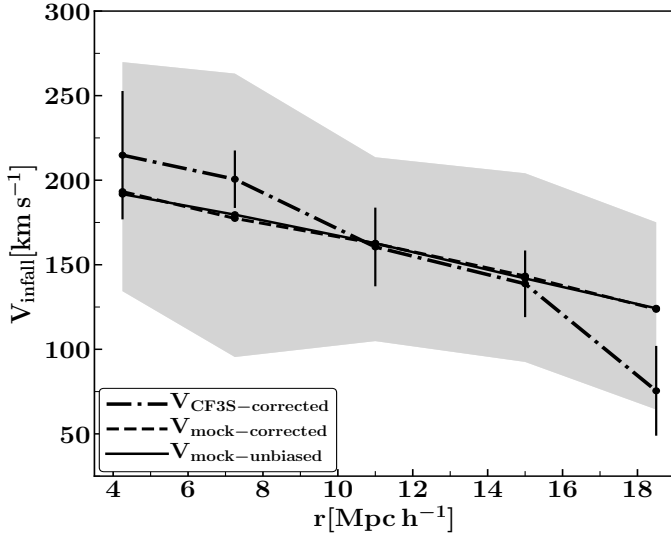


Fig. 6. Mean infall velocity as a function of distance to the group center for corrected samples. The dashed lines indicate the mean velocity obtained from the corrected mock catalogs, and the dot-dashed line corresponds to Cosmicflows-3 sample corrected (CF3S-corrected). The solid lines corresponds to the mean infall velocity for the mock-unbiased catalogs shown in solid lines of figure 5. Error bars correspond to the uncertainty in the VCF3S-corrected. The shaded regions indicate the variance obtain from 25 mock-corrected catalogs.

provide a good fit to the measured values of f for this group sample. The fitting parameters obtained for different subsamples provides the factors (f) used to correct the infall velocities measured (V_{CF3S}) in the corresponding CF3S. These observational flows corrected hereafter are called V_{CF3S} -corrected, in a similar way flows corrected on mock-biased catalogs are called V_{mock} -corrected. The corrected infall pattern derived from the CF3S is shown as dot-dashed lines in figure 6, the dashed line corre-

sponds to the average infall flow in 25 mock-corrected catalogs, and the solid line corresponds to the actual mean infall flow directly obtained from peculiar velocities in the mock-unbiased catalogs. The gray region enclose the 5 and 95 percentiles of the infall distribution on the 25 mock-corrected catalogs which can be taken as a measure of cosmic variance.

As can be seen in figure 6, there is a clear evidence of infall motions up to 16 $Mpc h^{-1}$. We also notice that V_{CF3S} -corrected and V_{mock} -corrected reaches 200 kms^{-1} at regions close to the groups ($\approx 4 Mpc h^{-1}$). The resulting mean velocities obtained here are consistent with those found by Ceccarelli et al. (2005). For larger distances to the groups the infall amplitude decreases down to about 120 kms^{-1} and infall uncertainties increases.

Here and throughout, we used the Kolmogorov-Smirnov (KS) test to find the statistical significance of the differences between infall velocity amplitudes for the different samples. We consider that the differences between distributions are highly significant if the p -value es $p < 0.01$.¹ The KS test confirms that the slope value of V_{CF3S} -corrected profile in figure 6 is significant at the 3 σ level.

These results are reasonable considering that close to the groups, galaxy peculiar velocities are dominated by the group potential well whereas at larger distances the surrounding large scale structure strongly affects the velocity field.

Taking into account our cosmic variance determinations, the mean infall velocities V_{CF3S} -corrected are consistent to those V_{mock} -corrected from mock-biased catalogs.

4.2. Dependencies on group properties

In this subsection, we analyze the characteristics of the peculiar velocity field around groups and its relation to group mass.

We subdivide the group sample according to mass estimated from the integrated K_s band luminosity (hereafter mass, M) into two group subsamples: groups with $M > 3.4 \times 10^{13} M_{\odot}$ and $M < 3.4 \times 10^{13} M_{\odot}$ dubbed high Mass (HM) and low Mass groups (LM) respectively. This limit was chosen in such way that each subsample contains a similar numbers of groups, as shown in table 1.

Similarly, we analyze the 25 mock catalogs and estimate the mean infall amplitude for galaxies in the mock-unbiased and mock-biased catalogs. This allows to infer the correction factors (f) for each sub-sample and use them to derive the true amplitudes of the infall velocity field in the observations. Here and throughout, observed mean infall velocities always refer to those corrected by the factor f in CF3S and the cosmic variance is obtained from the 25 mock-corrected catalogs.

The resulting relative amplitude of the radially inwards streaming motions are shown in figure 7. We show the ratio ($\frac{V_{HM}}{V_{LM}}$) between the infall amplitude of the two samples. As it can be seen in this figure, there is a clear difference in the mean infall amplitude onto group samples of high and low mass, the infall velocity amplitude associated to the high mass groups are systematically larger than that corresponding to low mass groups in the range of group centric distances explored. This behavior is stronger close to the center of the groups, where galaxies around high mass groups exhibit noticeably higher infall than galaxies around low mass groups. The KS test shows that the

¹ When we quote the statistical significance of a difference between two distributions (x_i and y_i), we compute $P(\Delta\chi^2, N_{dof})$ where $\Delta\chi^2 = \sum_i [d_i/\sigma(d_i)]^2$ with $d_i = (x_i - y_i)$ for each bin and $\sigma(d_i) = \sqrt{\sigma(x_i)^2 + \sigma(y_i)^2}$. Notice that $P(x, N)$ is a χ^2 distribution with N degrees of freedom.

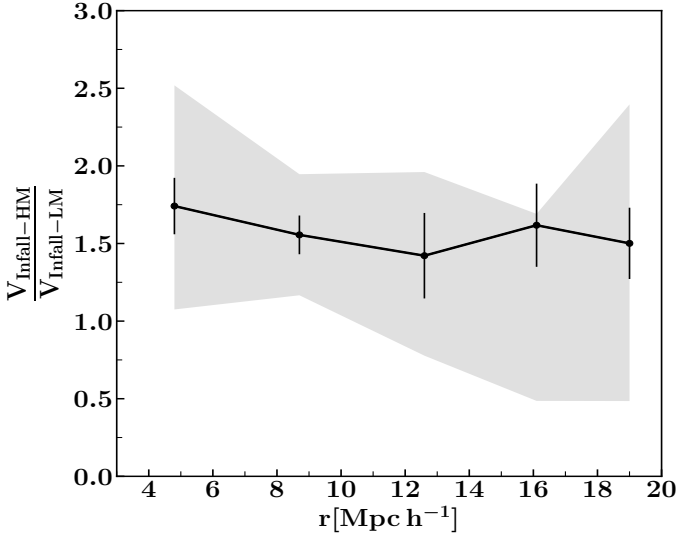


Fig. 7. The solid line shows the ratio of the mean infall velocity of high to low mass groups as a function of distance to the group centers in observational data. Error-bars indicate the uncertainty in the mean infall velocity and the gray shadow region shows the dispersion of 25 mock catalogs.

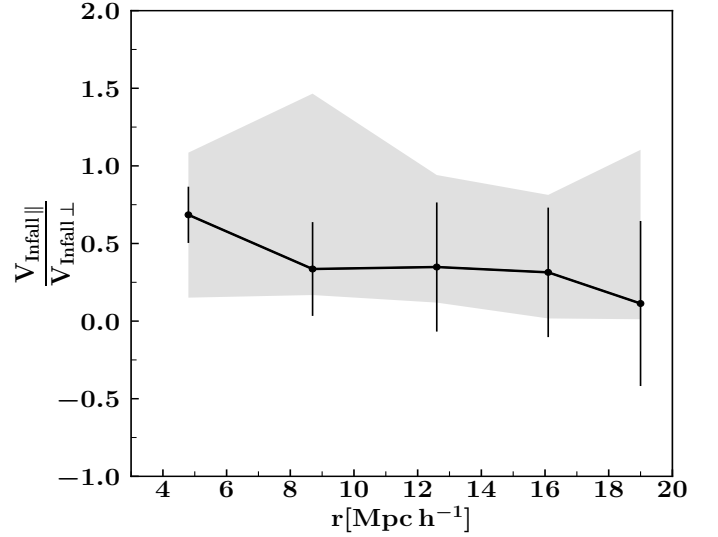


Fig. 8. Mean infall velocity ratio ($V_{\text{infall}\parallel} / V_{\text{infall}\perp}$) for groups with overdensities in the direction parallel and perpendicular to the LOS in the observational data. Error-bars indicate the uncertainty in the relative mean velocity and the gray shaded region shows the variance as in previous figures.

differences between infall velocity amplitudes are statistically significant ($p < 0.01$), consistent with a statistical confidence at the 3σ level. The gray shaded area in this figure corresponds to variance cosmic taken from the mock catalogs while error-bars indicate the relative uncertainty between both samples as derived from the linear fitting of peculiar velocities and $\cos(\theta)$.

Based on these studies, we adopt mass estimated from luminosity as a suitable indicator of group mass.

5. Large scale environment vs infall

5.1. Velocity field anisotropies

In a first approximation, the mean velocity field around groups of galaxies can be suitably described by the spherical infall model. The velocities predicted by this model are in qualitative agreement with our results (see figure 7 where the amplitude of the mean infall velocity field is strongly influenced by the group total mass). This model has also been successful in constraining group masses (Pivato et al. 2006) although we notice relevant departures from this simple picture given that the mass distribution around groups is strongly anisotropic due to the network of filaments, walls and clusters dominating the large scale Universe. For this reason the velocity fields surrounding groups exhibit a significant variance which is strongly connected to surrounding large scale structures (Kashibadze et al. 2020; Courtois et al. 2019; Tully et al. 2019; Libeskind et al. 2015). These effects have been reported and analyzed in numerical simulations (Ceccarelli et al. 2011) and in this work we aim at obtaining observational counterparts of these theoretical results.

Notice that since only the LOS component of observational peculiar velocities are available, the observational velocity field for groups with overdensities along the LOS can be strongly determined by galaxies residing in these filamentary regions. On the other hand, groups located in global overdensities perpendicular to the LOS may have galaxies with velocity dominated by flows from underdense regions onto groups. In this section we examine these different cases by analysing the derived infall flow from over/under-dense regions by selecting two samples

of groups with large scale surrounding regions parallel and perpendicular to the line of sight. In order to perform this test we compute the density in a spherical region of radius 15 Mpc h^{-1} centered in the groups and consider separately the regions close to the LOS, $\theta < \frac{\pi}{6}$, and perpendicular to it $\frac{\pi}{3} < \theta < \frac{2\pi}{3}$. This allows to separate the total subsample into two groups, those with predominant LOS overdensities (\parallel), and those predominant overdensities in the plane of the sky (\perp). The number of groups for each sample is stated in table 1.

With the aim at shedding light on the anisotropic infall onto groups in the observations, we estimate the mean velocity field around the two samples of groups. Applying a similar analysis to that performed in the previous subsection we compute the ratio between both subsamples, and show the results in figure 8. As it can be noticed, mean velocities are significantly different as inferred from the KS test which gives a high statistical significance at more than the 5σ level. The ratio $V_{\text{infall}\parallel} / V_{\text{infall}\perp}$ for the two group samples remains below 1 (solid line, $V_{\text{infall}\parallel} > V_{\text{infall}\perp}$), indicating that the streaming motion of galaxies onto groups with large underdense regions is faster than those of galaxies from global overdensities. This result is in sync with Pereyra et al. (2019); Mahajan et al. (2012); Ceccarelli et al. (2011), which showed that a relatively high galaxy density in the infalling regions of groups promotes tidal interactions with neighboring galaxies, resulting in a smaller magnitude of the velocities along these high density regions. We stress the fact that both sub-samples of groups have similar mass, and luminosity distributions so that these differences should be owed to an environment difference.

5.2. Overall density around groups

The spherical infall model assumes an isotropic mass distribution of groups as well as their isolation so that infall pattern is associated to an isotropic convergent velocity field. Given that groups of galaxies are not isolated but immersed in the cosmic web, local irregularities can affect the local dynamics and even more, large scale bulk motions may imprint significant peculiar

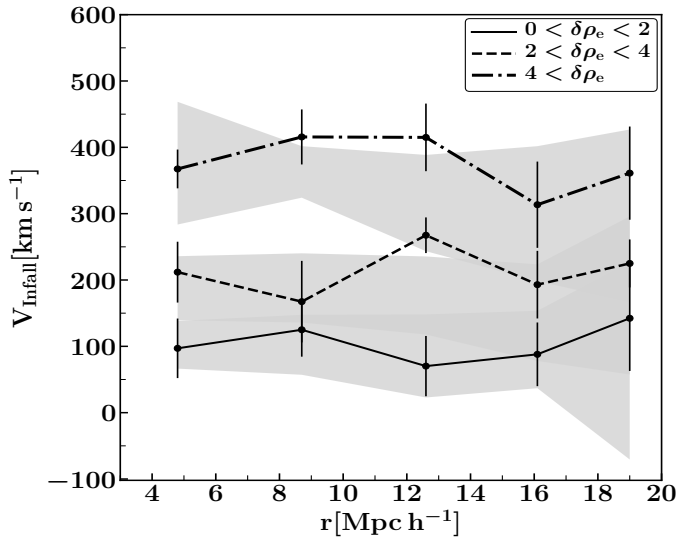


Fig. 9. Dependence of infall onto groups from regions with different density environments in observational data. The lines correspond to the mean infalling velocity onto groups embedded in regions with $\delta\rho_e > 4$ (dot-dashed); $2 < \delta\rho_e < 4$ (dashed), and $0 < \delta\rho_e < 2$ (solid). The three gray shaded regions represent the variance from equivalent high, medium and low density environment in the mock catalogs respectively. Error-bars correspond to the uncertainties in the derived mean infalling velocities.

velocities to the galaxies beyond the small/intermediate effects associated to the galaxy groups (Kitaura et al. 2012; Hoffman et al. 2018; Graziani et al. 2019).

We have analyzed the effects of the surrounding density field around groups on the infalling velocity pattern by selecting three subsamples of groups embedded in under/intermediate/over dense regions. For the environment characterization, we have computed the integrated galaxy overdensity on a region from 5 Mpc h^{-1} to 10 Mpc h^{-1} ($\delta\rho_e$) centered in the group and we have estimated the mean velocities as a function of group-centric distance for each sample.

The low density subsample is defined by $0 < \delta\rho_e < 2$, the intermediate density subsample, by $2 < \delta\rho_e < 4$, and the high density subsample, by $\delta\rho_e > 4$.

In figure 9 we show the resulting infall velocity pattern derived from the three group subsamples that consider their mean surrounding density. Solid line corresponds to $0 < \delta\rho_e < 2$, dashed line to $2 < \delta\rho_e < 4$ and dot-dashed line to $\delta\rho_e > 4$.

As it can be seen in this figure, groups in all density environments show systematic infalling velocities over all range of distances explored with increasing amplitude for higher density environments. In figure 9 it can be appreciated that as the density environment around groups increases, the amplitude of the streaming infall velocity field increases as well. The KS tests confirm that the differences among infall velocity amplitudes of high, intermediate and low density environment are statistically significant at a very high confidence level ($> 3\sigma$ for all samples). As expected, we find a strong dependence of the velocity field around groups on both group mass and surrounding mass density at significantly large scales (Einasto et al. 2005, 2003b).

6. Local vs global velocity fields

Several works (e.g. Einasto et al. 2003b,a, 2005; Lietzen et al. 2012) have shown that groups and clusters of galaxies in high

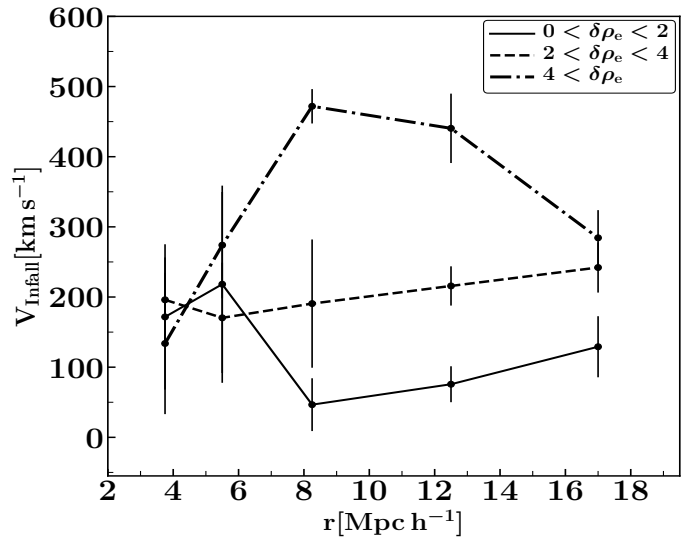


Fig. 10. Same as figure 9 with observational group subsamples restricted to have a similar mass distribution. The line types correspond to the same environmental density ranges analyzed in figure 9. Error-bars indicate the uncertainty in the mean infalling velocities.

density regions are richer, more massive, and more luminous than groups and clusters of galaxies in low density regions. In this context, the results obtained in the previous section could be biased by the inclusion of samples of different mass groups. Therefore, in this section we examine the inferred mean infall pattern considering separately the effects of group mass and environment.

6.1. Density around groups

We restrict the sample construction so that the groups have comparable statistical properties associated to mass. Given that we select samples of groups with similar statistical properties, the possible differences of their velocity fields should be associated only to environment.

We select three subsamples of groups having similar mass (and luminosity) distributions and embedded in regions of different overall galaxy density bins, where these density bins correspond to those in subsection 5.2. Since the mass distribution of the three subsamples are similar, we expect similar contributions to the mean infall by the group itself. Therefore, the differences between the resulting velocity field of the two samples can be associated to the difference imposed by the surrounding environment. In figure 10 we show the mean infall amplitude as a function of group-centric distance for groups in different galaxy density environments, solid lines $0 < \delta\rho_e < 2$, dashed line $2 < \delta\rho_e < 4$ and dot-dashed line $\delta\rho_e > 4$. As it can be seen in the figure the velocities are comparable for distances to the group centre smaller than $\sim 6 \text{ Mpc h}^{-1}$ where the infall amplitude rises to $V_{\text{infall}} \approx 200 \text{ km s}^{-1}$ at $r \approx 6 \text{ Mpc h}^{-1}$. This is consistent with the fact that the three samples have a comparable mass distribution. So, the effect of similar group masses on the surrounding velocity field can be clearly appreciated. On the other hand, in figure 10 it can be noticed that the velocity curves differ significantly at large separations ($r > 8 \text{ Mpc h}^{-1}$), with associated KS test p-values < 0.01 . These results show the impact of the large scale environment on the velocity field, in agreement with previous works (Einasto et al. 2005; Lietzen et al. 2012).

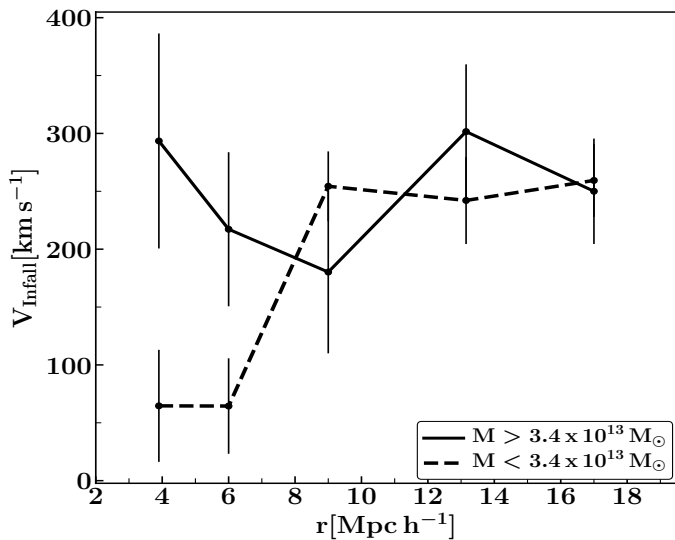


Fig. 11. Infall dependence on group mass in the observational data. The group subsamples are restricted to reside in similar density environments ($1 < \delta\rho_e < 2.5$). The solid (shaded) line corresponds to high (low) mass groups (M larger (smaller) than M_{median}). Error-bars represent the uncertainty in the derived mean infalling velocities.

6.2. Group mass dependence

Once examined the effect of the global overdensity on the velocity field around poor galaxy groups, here we explore the contribution of group mass to the velocity field in an environment controlled subsample. We restrict the sample of groups to those residing in global environments within a restricted galaxy overdensity ($1 < \delta\rho_e < 2.5$) corresponding to the 25 and 75 percentiles and comprises the 50% of the total group sample. Within this constraint, we select two subsamples of groups with mass larger/smaller than the total sample median mass ($\approx 3.4 \times 10^{13} M_{\odot}$). The mean/median mass for the larger (smaller) subsample is $10.4 \times 10^{13}/6.74 \times 10^{13} M_{\odot}$ ($18.8 \times 10^{12}/17.8 \times 10^{12} M_{\odot}$), with mean/median mass ratios 5.5/3.7.

Given that we select the two subsamples of groups in similar large-scale environments, any differences on the peculiar velocity field should be attribute to the group mass.

We derive the mean infall amplitude for the two subsamples and show the results in figure 11, where solid (dashed) line corresponds to group masses larger (lower) than the median. As it can be noticed in this figure, high and low mass groups exhibit mean infall amplitudes clearly distinguishable closer to the group ($r < 8 \text{ Mpc h}^{-1}$): infall amplitude reaches 300 km s^{-1} for high mass groups (solid line) and remains below 100 km s^{-1} for low mass groups (dashed line) at the smallest group-centric distances analyzed ($\sim 4 \text{ Mpc h}^{-1}$). The KS test shows that, up to 8 Mpc h^{-1} , the differences between the infall velocity amplitudes of these samples are statistically significant at the 2.5σ level. Consequently, the infall amplitude ratio of high-mass to low-mass groups is a factor 4.5 ± 1.0 in this close surroundings of groups, consistent with the mass ratio values (5.5 mean, 3.7 median) of the two group subsamples. This ratio is in very good agreement with the linear infall model predictions for the velocity field.

As it can be noticed in the figures 10 and 11 we can easily distinguish two regimes characterizing the peculiar velocity field at small and large scales.

7. Discussion

Galaxy peculiar velocities originate in departures of motions from a pure Hubble flow induced by irregularities of the mass distribution at large scales. These motions have a statistical imprint in the redshift-space distortions of the two point correlation function and provide useful information on the global dynamics. However, peculiar velocities can be directly estimated through redshift independent distance indicators and may be used to extract useful information on the dynamics of galaxies and galaxy systems besides the correlation function analysis. Since peculiar velocity measurements provide a direct trace of the mass distribution there are no issues regarding galaxy bias which add complexity in redshift-space correlation analysis. For this reason, direct estimates of galaxy peculiar velocities may provide useful cosmological test in forthcoming surveys with more accurate determinations in the local Universe. In this work we have focused our analysis on the measurements of infall of galaxies onto groups, and its dependence on group mass and environment. Since groups of galaxies are part of the cosmic web, the local dynamics cannot be simply addressed through a spherical infall model given that large scale bulk motions affect the local effects associated to group mass overdensities.

Firstly we apply the spherical infall model to derive the mean infall velocity pattern onto groups of different characteristics. Since only the line-of-sight projection of galaxy peculiar velocities can be obtained, the derived infall velocity field relates to galaxy positions relative to both the group center and the observer (see equation 2). Present data are affected by large distance measurement uncertainties which lead to large peculiar velocity errors. This fact is associated to the presence of systematic effects of distance estimates that can bias the inferred velocity field. To properly address the impact of distance measurement uncertainties on the mean infall mean velocity determination by assigning suitable errors to mock catalogs constructed similar to observations

We obtain accurate determinations of the mean infall velocity profile around groups of different mass range and in different environments which exhibit amplitudes in the range 200 to 350 km/s, entirely consistent with numerical simulation results.

We have extended our work by considering the impact of large-scale environment on the mean infall galaxy velocity onto groups.

We compare the effects of large-scale inhomogeneities around galaxy groups on the mean infall velocity, finding these effect significantly smaller along the direction of high density enhancement compared to those along low density. This provides evidence that groups grow in a different fashion from filaments than elsewhere. These results are in agreement with previous studies of the environmental effects on groups and clusters growing by mass accreted from their surrounding structures ranging from isolated galaxies to large groups which merge to form larger systems (McGee et al. 2009). McGee et al. (2009) results also show that a large fraction of galaxies accreted onto clusters were formerly in groups.

We obtain a significant dependence of the mean infall pattern on the group large-scale environment consistent with higher infall velocities onto groups residing in large overdense regions.

We recall that infall models are mainly based on assumptions of spherical symmetry onto an isolated mass overdensity. This simplified scenario may have an impact on total group mass determinations taking into account our studies of the streaming motions dependence on global density environment and anisotropic mass distribution around groups in observations.

Due to upcoming improvement on observational data and peculiar velocity precision, studies such as those presented in this work may provide aid in our current understanding of the growth of structures in the Universe.

Acknowledgements. This work has been partially supported by Consejo de Investigaciones Científicas y Técnicas de la República Argentina (CONICET), and the Secretaría de Ciencia y Técnica de la Universidad Nacional de Córdoba (SeCyT).

References

- Adams, C. & Blake, C. 2020, *MNRAS*, 494, 3275
- Cai, Y.-C., Taylor, A., Peacock, J. A., & Padilla, N. 2016, *MNRAS*, 462, 2465
- Ceccarelli, L., Padilla, N. D., Valotto, C., & Lambas, D. G. 2006, *MNRAS*, 373, 1440
- Ceccarelli, L., Paz, D. J., Padilla, N., & Lambas, D. G. 2011, *MNRAS*, 412, 1778
- Ceccarelli, M. L., Valotto, C., Lambas, D. G., et al. 2005, *ApJ*, 622, 853
- Colin, J., Mohayaee, R., Sarkar, S., & Shafieloo, A. 2011, *MNRAS*, 414, 264
- Courtois, H. M., Kraan-Korteweg, R. C., Dupuy, A., Graziani, R., & Libeskind, N. I. 2019, *MNRAS*, 490, L57
- Croft, R. A. C., Dalton, G. B., & Efstathiou, G. 1999, *MNRAS*, 305, 547
- Dekel, A. 1994, *ARA&A*, 32, 371
- Desjacques, V. & Sheth, R. K. 2010, *Phys. Rev. D*, 81, 023526
- Diaferio, A. 1999, *MNRAS*, 309, 610
- Diaferio, A. & Geller, M. J. 1997, *ApJ*, 481, 633
- Dupuy, A., Courtois, H. M., & Kubik, B. 2019, *MNRAS*, 486, 440
- Einasto, J., Hütsi, G., Einasto, M., et al. 2003a, *A&A*, 405, 425
- Einasto, J., Tago, E., Einasto, M., et al. 2005, *A&A*, 439, 45
- Einasto, M., Einasto, J., Müller, V., Heinämäki, P., & Tucker, D. L. 2003b, *A&A*, 401, 851
- Eke, V. R., Frenk, C. S., Baugh, C. M., et al. 2004, *MNRAS*, 355, 769
- Feldman, H. A., Watkins, R., & Hudson, M. J. 2010, *MNRAS*, 407, 2328
- Graziani, R., Courtois, H. M., Lavaux, G., et al. 2019, *MNRAS*, 488, 5438
- Henriques, B. M. B., White, S. D. M., Thomas, P. A., et al. 2015, *MNRAS*, 451, 2663
- Hoffman, Y., Carlesi, E., Pomarède, D., et al. 2018, *Nature Astronomy*, 2, 680
- Huchra, J. P., Macri, L. M., Masters, K. L., et al. 2012, *ApJS*, 199, 26
- Huterer, D., Shafer, D. L., Scolnic, D. M., & Schmidt, F. 2017, *J. Cosmology Astropart. Phys.*, 2017, 015
- Johnson, A., Blake, C., Koda, J., et al. 2014, *MNRAS*, 444, 3926
- Kashibadze, O. G., Karachentsev, I. D., & Karachentseva, V. E. 2020, *A&A*, 635, A135
- Kim, A. G. & Linder, E. V. 2020, *Phys. Rev. D*, 101, 023516
- Kitaura, F.-S., Erdoğan, P., Nuza, S. E., et al. 2012, *MNRAS*, 427, L35
- Lavaux, G., Tully, R. B., Mohayaee, R., & Colombi, S. 2010, *ApJ*, 709, 483
- Libeskind, N. I., Hoffman, Y., Tully, R. B., et al. 2015, *MNRAS*, 452, 1052
- Lietzen, H., Tempel, E., Heinämäki, P., et al. 2012, *A&A*, 545, A104
- Ma, Y.-Z. & Pan, J. 2014, *MNRAS*, 437, 1996
- Mahajan, S., Raychaudhury, S., & Pimblett, K. A. 2012, *MNRAS*, 427, 1252
- McGee, S. L., Balogh, M. L., Bower, R. G., Font, A. S., & McCarthy, I. G. 2009, *MNRAS*, 400, 937
- Nusser, A. & Davis, M. 2011, *ApJ*, 736, 93
- Padilla, N. D., Merchán, M. E., Valotto, C. A., Lambas, D. G., & Maia, M. A. G. 2001, *ApJ*, 554, 873
- Paz, D., Lares, M., Ceccarelli, L., Padilla, N., & Lambas, D. G. 2013, *MNRAS*, 436, 3480
- Peebles, P. J. E. 1976, *ApJ*, 205, 318
- Peebles, P. J. E. 1980, *The large-scale structure of the universe*
- Pereyra, L. A., Sgró, M. A., Merchán, M. E., Stasyszyn, F. A., & Paz, D. J. 2019, *arXiv e-prints*, arXiv:1911.06768
- Pivato, M. C., Padilla, N. D., & Lambas, D. G. 2006, *MNRAS*, 373, 1409
- Planck Collaboration, Ade, P. A. R., Aghanim, N., et al. 2011, *A&A*, 536, A1
- Regos, E. & Geller, M. J. 1989, *AJ*, 98, 755
- Springel, V., White, S. D. M., Jenkins, A., et al. 2005, *Nature*, 435, 629
- Strauss, M. A. & Willick, J. A. 1995, *Phys. Rep.*, 261, 271
- Tonegawa, M., Park, C., Zheng, Y., et al. 2020, *arXiv e-prints*, arXiv:2005.12159
- Tully, R. B. 2015, *AJ*, 149, 171
- Tully, R. B., Courtois, H. M., Dolphin, A. E., et al. 2013, *AJ*, 146, 86
- Tully, R. B., Courtois, H. M., & Sorce, J. G. 2016, *AJ*, 152, 50
- Tully, R. B., Pomarède, D., Graziani, R., et al. 2019, *ApJ*, 880, 24
- Turnbull, S. J., Hudson, M. J., Feldman, H. A., et al. 2012, *MNRAS*, 420, 447
- Watkins, R., Feldman, H. A., & Hudson, M. J. 2009, *MNRAS*, 392, 743